

An Analytical Model for Predicting Stab Resistance of Flexible Woven Composites

Limin Hou · Baozhong Sun · Bohong Gu

Received: 18 July 2012 / Accepted: 21 August 2012 / Published online: 2 September 2012
© Springer Science+Business Media B.V. 2012

Abstract Flexible woven composites have been widely used in geotextiles and light weight building structures. The stab resistance behavior of the flexible woven composite is an important factor for the application design. This paper reports an analytical model for predicting stab resistance of flexible woven composites under perpendicular stab with a blunt steel penetrator. The analytical model was established based on the microstructure and the deformation shape of the flexible woven composite under normal penetration. During the quasi-static stab penetration, the strain energies of warp and weft yarns and resins have been calculated. The stab resistance was calculated from the strain energies of the flexible woven composite. Furthermore, the contributions of the warp and weft yarns, resins to the stab resistance have been analyzed. It was found the three constituents have near the same contribution to the stab resistance. The higher value of weaving density, strength of yarns and especially the higher strength coating resins will lead the higher stab resistance. With the analytical model, the stab resistance would be expected to be designed in an efficient way with an acceptable precision.

Keywords Flexible woven composite · Fabric architecture · Stab resistance · Strain energy

Nomenclature

r	radius of the clamping fixture
W	width of the stab
T	thickness of the stab
x	the displacement of the stab during the stab process
x_s	the rise height of the secondary yarns as the stab goes up to x
d	space between the adjacent yarns
l	the original length of the yarn
la	the length of the yarn after elongating
T_m	thickness of the flexible woven composite
Nt	linear density of the yarn
E	modulus of the yarn
A	cross-section area of yarn

L. Hou · B. Sun · B. Gu (✉)
College of Textiles, Key laboratory of high-performance fibers & products, Ministry of Education,
Donghua University, Shanghai, China 201620
e-mail: gubh@dhu.edu.cn

V	volume of the material
ε	strain of the material
σ	stress of the material
e	strain energy stored by the material during the stab process
F	the force applied on the material during the stab process

1 Introduction

Lightweight flexible woven composites with high strength have great potential applications to geotextiles, light structure building, oil plants transportation etc. The flexible woven composites are often suffered from the stab or puncture damage in the service life caused by the sharp objects or rocks. The flexible woven composites consist of at least two components: base fabric and coating resin. The main purpose of the base fabric is to provide strength and dimensional stability to the coated fabric structure. Coating protects the base fabric against the outside effects while making the structure air and water proof. How to relate the stab resistance with the mechanical behaviors of fabrics and coating resins is the key to design a higher stab resistance flexible woven composite in an efficient way. From the appropriate choices of fabrics and coating resins and the fabric structures, the stab resistance of the flexible woven composite could be optimized. The objective of this investigation is to find the relationship between the stab resistance and the properties of fibers, resins and the microstructures of flexible woven composites in an analytical way. From the analytical model, the influence of the structure parameters on the stab resistance will be revealed to extend the design of the flexible woven composites with higher stab strength.

The stab resistance of flexible textile composite has been investigated in experimental and theoretical approaches. In experimental, the stab resistance of flexible textile composites was tested with different shaped probe tip to show the stab strength of different structural flexible textile composites. For example, Nguyen[1] demonstrated the maximum stab force depends on the contact surface between the elastomeric membrane and the probe tip. Kim[2] evaluated the stab resistance behavior against different shapes of impactors and showed three distinctive steps for the p-aramid fabrics against a knife impactor. Ghosh[3] tested the puncture resistance of geotextiles under uniform radial pre-strain. Mayo[4] found that thermo-plastic laminated fabrics will have higher stab resistance through a combination of increased cut resistance and reduced windowing. Baucom and Zikry[5] indicated that the 3D laminates consistently had greater damage tolerance than the 2D laminates and the 3D monolithic composites. Yang[6] investigated the effect of orientation by solid-state cross-rolling on the morphology stab deformation and fracture mechanism of an amorphous TROGAMZD material and three semi-cry stalling polymers. Tien[7] evaluated the anti-stabbing performance of fabric layer woven with various hybrid yarns under different fabric conditions. Chen[8] investigated the manufacturing and stab resistance properties of compound fabric reinforced using recycled nonwoven selvages. Flambard[9] showed the excellent stab performance of PBO in comparison with PPT. Brachman[10] investigated the stab performance of geo-membrane and the influences of applied pressure, clay water content, stone size, stone burial depth and protection layer on the geo-membrane tensile strains. Beiermann[11] manufactured a flexible self-healing system capable of healing stab damage and found that it increased with composite layer thickness, and decreased with increasing stab hole size. Segreti[12] studied the stab failure mode of PMMA at low and high velocities experimentally. Hosur[13] investigated static and dynamic stab resistant properties of the TP-Kevlar composites and the results demonstrated that the TP-Kevlar composite targets

showed more resistance to quasi-static spike testing than quasi-static knife testing. Decker[14] investigated the stab resistance of Kevlar (R) and Nylon fabrics treated with shear thickening fluid (STF) and the results indicated that these novel materials could be used to fabricate flexible body armors that provide improved protection against stab threats. The above-mentioned references have concerned with the stab failure of the different kinds of flexible textile composites under sharp probe tip or knives. This kind of sharp penetrator can not simulate the stab damage of the flexible woven composites under rocks or rigid sands. In order to reveal the stab damage of the flexible pipeline or architecture membrane during the service life, the stab damage under blunt penetrator should be tested. Here a blunt steel penetrator will be used to test the stab damage of flexible woven composites.

In theoretical, Termonia[15] developed a comprehensive model first to analyze the factors controlling the resistance of fiber fabric systems against needle stab and to simulate the damage process under stab loadings. Lee[16] assessed the penetration failure mechanisms of armor-grade fiber-reinforced composites with low resin content and they utilized numerical modeling to show that yarn slippage in fabrics resulted in a smaller effective penetrator radius leading to a decrease in energy absorption capacity with equal penetrator masses. Recently numerical methods (for example, Finite Element Analyses) were introduced to simulate the stab progress of woven fabrics[17, 18]. All these theoretical investigations revealed the stab damage mechanisms and stab energy absorptions of the flexible woven composite under puncture loading. With these theoretical models, the stab resistance could be designed before the manufacturing. However, all these models have not presented the relationships between the stab resistance, and the microstructures and the behaviors of constituent materials. Furthermore, all these models were not focused on the stab resistance under the blunt penetrator and should also to be simplified for fabric construction design.

Accompanied with our previous researches[17, 18], this paper will report an analytical model to describe the deformation/damage mechanism flexible woven composite under stab loading with a blunt penetrator. An analytical model has been established on the strain energy principle to predict load–displacement behavior of the flexible woven composite. The stab responses and damage morphology of flexible woven composite samples were obtained from the stab testing. The agreement between the theoretical and experimental proves the validity of the analytical model. With the analytical model, the stab resistance of flexible woven composite could be designed in a convenient way and also in an acceptable precision compared with that of finite element analyses model.

2 Materials and Experimental

2.1 Flexible Woven Composite

The flexible woven composite chosen for stab testing was 2/1 twill woven fabric coated with TPU (thermoplastic urethane) resin. The woven fabric was woven using PET continuous filament tows. The specifications of the yarns, the woven fabric and the TPU resin are listed in Tables 1, 2 and 3 respectively. Figure 1 shows the cross-sectional photographs of the flexible woven composite in warp and weft directions. The interface between the fabric and the matrix are shown in Fig. 2 after peeling off the coating layer. It can be found that there was little penetration of the TPU resin into the fabric.

Table 1 Parameters of the warp and weft yarns

Yarn	Linear density (Tex)	Modulus (GPa)	Volume density (g/cm ³)	Cross-section area (mm ²)
Warp	454×2	7.32	1.38	1.014
Weft	700×2	6.97	1.38	0.658

2.2 Quasi-Static Stab Tests

As is shown in Fig. 3, the quasi-static stab tests of the flexible woven composite were conducted on MTS-810 testing machine. The environment for all the tests was maintained at a relative humidity of $65\pm 4.0\%$ and a temperature of $20\pm 2.0\text{ }^{\circ}\text{C}$, as recommended by ISO 139–2005. The schematic diagram of the quasi-static stab process is shown in Fig. 4. The specimen was fixed between two pieces of steel rings with an inner diameter of 12 cm. Three bolts and the concave/convex grooves on the inner face of the steel rings prevented the slippage of the specimen during the stab progress. The steel penetrator shape could effectively simulate the sharp objects like rocks which often stab the flexible oil pipelines or flexible architecture membranes. Specifications of the steel penetrator are shown in Fig. 5. The specimen was stabbed by the steel stab with a velocity of 100 mm/min. Damage morphology of the specimen is displayed in Fig. 6. The load–displacement curve obtained from the quasi-static stab test is shown in Fig. 7. It can be seen that the maximum displacement of the steel stab was 19 mm and the maximum force was 2,039 N during the specimen failure.

3 Analytical Modeling

3.1 Geometrical Model for the Woven Reinforcement

As observed from the deformation and damage morphology shown in Fig. 6, only the yarns directly in contact with the penetrator would be fractured, while the other yarns in the deformation region only have elongation. The yarns in the deformation region could be divided into two categories, one is the principal yarns which are contact with the penetrator during stab and another is the secondary yarns which are not contact with the penetrator in stab. Figure 8 depicts the deformation of the flexible woven composite in experimental and analytical model. The yarns are not straight but in a curved line which is caused by the uneven distribution of stress.

The principal yarns directly in contact with the penetrator will be broken first during stab because of the much lower failure strain than the TPU matrix and the

Table 2 Specifications of the woven fabric

Structure	Material	Areal density (g/m ²)	Warp density (ends/5 cm)	Weft density (ends/5 cm)
2/1 twill	Polyester	920	28	17

Table 3 Specifications of the TPU matrix

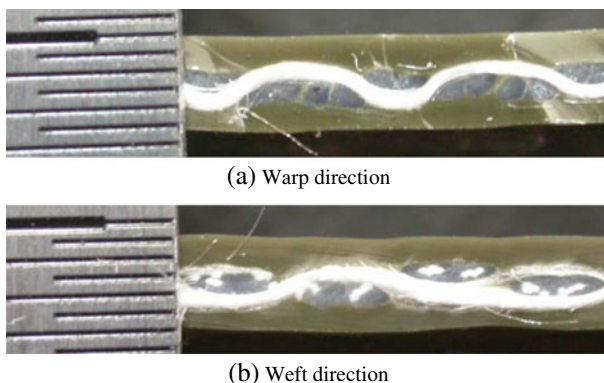
Coating material	Thickness (mm)	Areal density (g/m ²)	Modulus (GPa)
TPU	2.2	2950	14

higher stress than the secondary yarns. The principal yarns play an important role in improving the stab strength. From Fig. 8, we assume that the deformation shape of the principal yarns is an arc of a circle in geometrical model. The weft yarn was chosen as an example shown in Fig. 9. The grey part represents the steel penetrator and point A is the boundary point of the deformation region. The straight line OA (O is the center of the circle) is always perpendicular to the y-axis and the circle is always tangent to the y-axis during the stab process. Point B is the cross-point of the arc and the penetrator. The arc between point A and point B displays the deformation of the weft principal yarns under the stab. As observed from Fig. 10a, the principal yarns bend more and more as the stab displacement increases. Figure 10b shows that with the steel penetrator stabbing deeply, the center of the circle falls. The circle becomes small and hence the curvature of the circle decreases. By comparing Fig. 10a and b it could be found that there is a good agreement for the deformation of the flexible woven composite between experimental and analytical.

As shown in Fig. 6, only the principal yarns were fractured, while the secondary yarns in the deformation region only have elongation. The force applied on the secondary yarns is relatively smaller than that on the principal yarns. To simplify the analytical model, the secondary yarns were assumed to remain straight in the whole stab process, as shown in Fig. 12.

3.2 Numerical Calculations for the Woven Structure

A cartesian coordinate system was built as shown in Fig. 9. Subscripts j, w, m and c were defined to represent the warp yarns, the weft yarns, the matrix and the flexible woven composite respectively in the following calculation. When the steel stab stabbed to a depth of x , point A, B and O could be expressed as: $A(r, 0)$, $B(\frac{W}{2}, x)$, $O(r, x_0)$. According to the

**Fig. 1** Cross-sections of the flexible woven composite

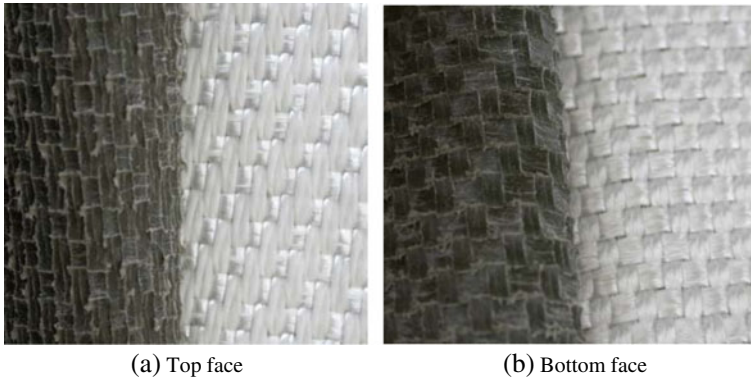


Fig. 2 Photographs of the flexible woven composite after peeling the coating layer off

nature of the circle ($OA=OB$), the relationship between x and x_0 could be obtained as follows:

$$x_0 = \frac{(2r - W)^2}{8x} + \frac{x}{2} = \frac{(2r - W)^2 + 4x^2}{8x} \quad (1)$$

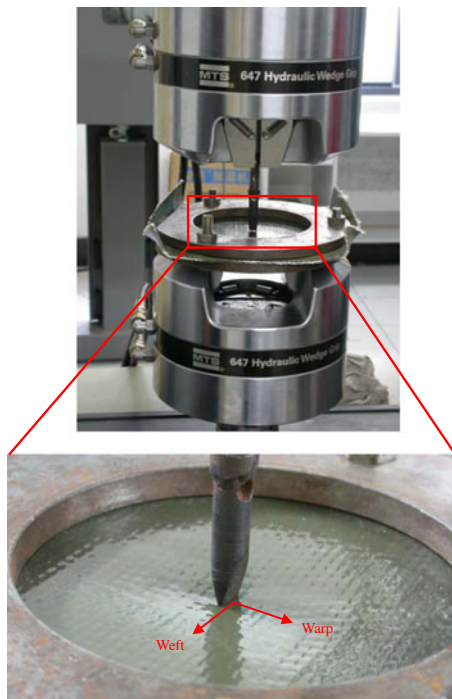


Fig. 3 Quasi-static stab tests on MTS 810.23 materials tester system

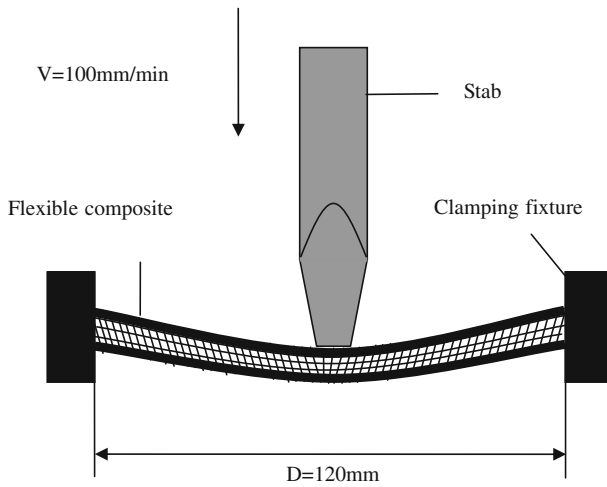


Fig. 4 Schematic diagram of the stab process

The expression of the circle is

$$x' = \frac{(2r - W)^2 + 4x^2}{8x} - \sqrt{\left(\frac{(2r - W)^2 + 4x^2}{8x}\right)^2 - (y' - r)^2} \tag{2}$$

When the stab goes up to x the height of the i th warp yarn could be obtained as:

$$x_{sj} = \frac{(2r - W)^2 + 4x^2}{8x} - \sqrt{\left(\frac{(2r - W)^2 + 4x^2}{8x}\right)^2 - (i \cdot d_j - r)^2} \tag{3}$$

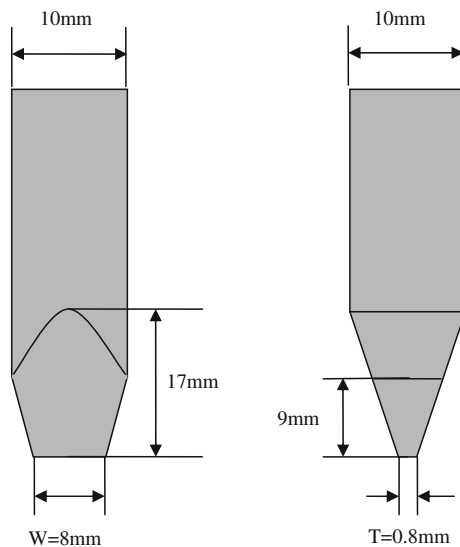


Fig. 5 Specification of the stab

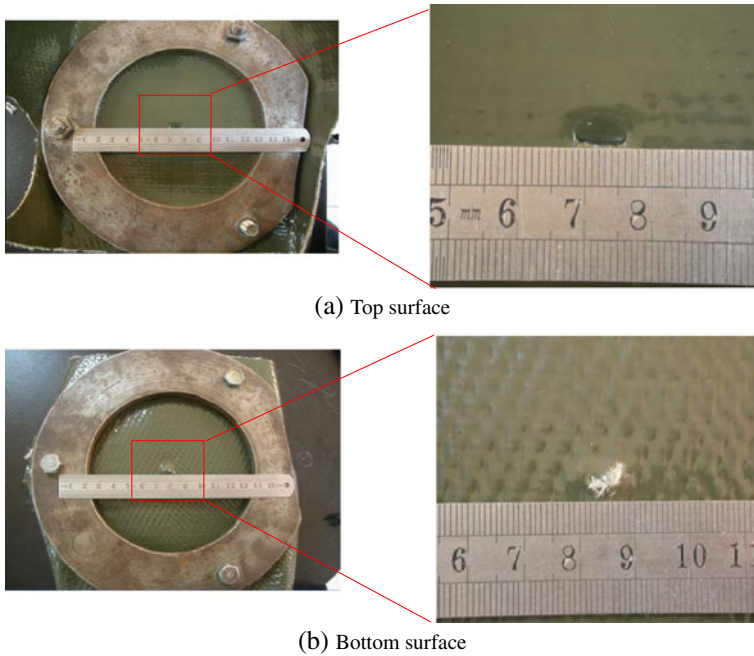


Fig. 6 Damage morphology of the specimen

According to the geometrical relationship, the length of the line segment AC is

$$L_{AC} = \frac{1}{2}L_{AB} = \frac{1}{2}\sqrt{\left(r - \frac{W}{2}\right)^2 + x^2} = \frac{\sqrt{(2r - W)^2 + 4x^2}}{4} \tag{4}$$

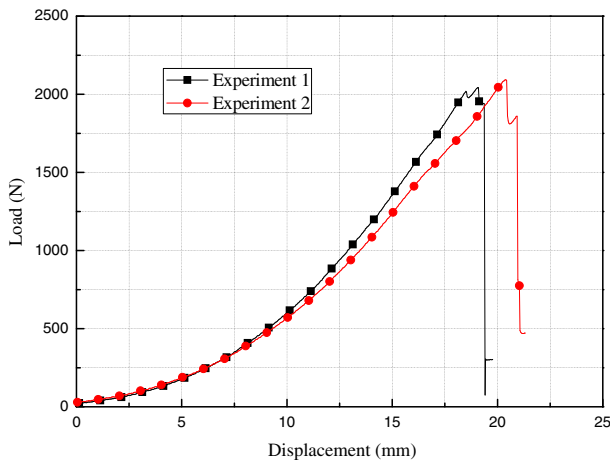
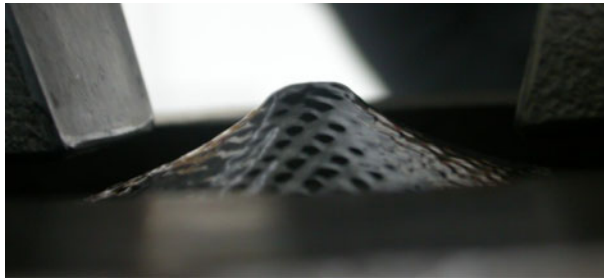
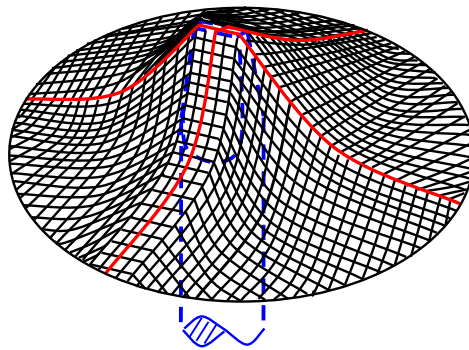


Fig. 7 Load–displacement curves of the specimen under stab load in experimental tests



(a) Experimental



(b) Theoretical

Fig. 8 Deformation of the flexible woven composite under stab load

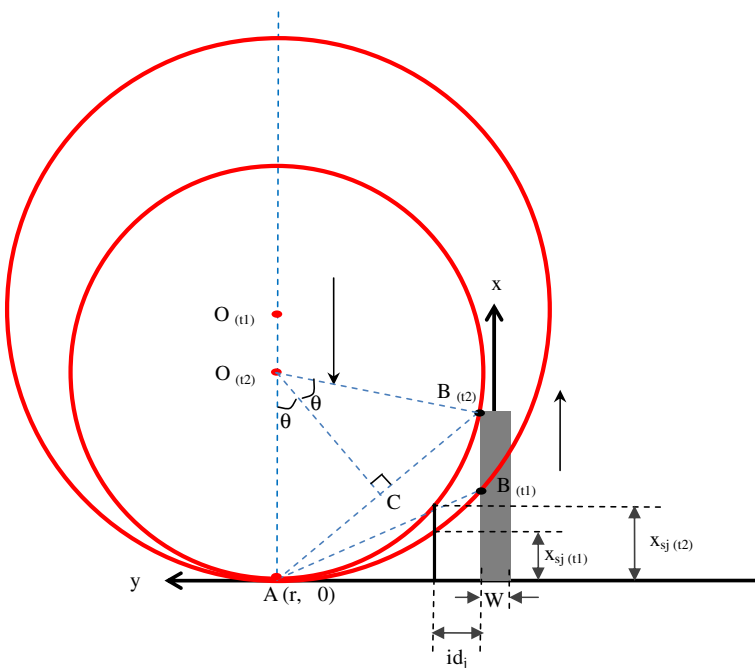
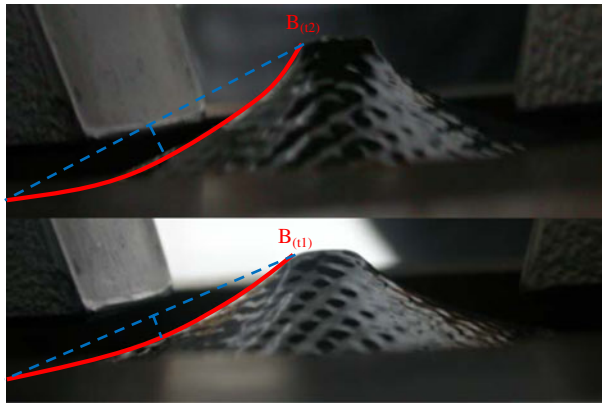
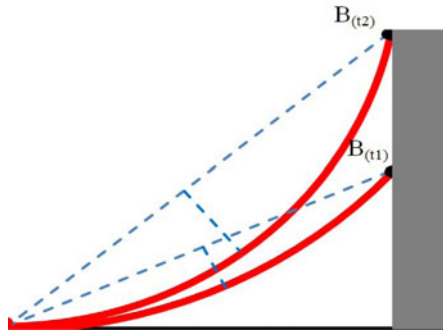


Fig. 9 Deformation evolution of the principal yarn during stab process



(a) Experimental tests



(b) Analytical model

Fig. 10 Comparison in the deformation of the specimen between experimental tests and analytical model

From the law of sines we can get

$$\sin \theta = \frac{L_{AC}}{x_0} = \frac{2x}{\sqrt{(2r - W)^2 + 4x^2}} \tag{5}$$

Then the length of arcAB is

$$|arcAB|_w = \frac{2\theta}{360^\circ} \cdot 2\pi x_0 = 2x_0\theta = \frac{(2r - W)^2 + 4x^2}{4x} \cdot \arcsin\left(\frac{2x}{\sqrt{(2r - W)^2 + 4x^2}}\right) \tag{6}$$

Arc AB shows half the w0 yarn under puncture load, so the length of half the w0 yarns after elongating could be calculated from Formula(7).

$$la_{w0} = \frac{(2r - W)^2 + 4x^2}{4x} \cdot \arcsin\left(\frac{2x}{\sqrt{(2r - W)^2 + 4x^2}}\right) \tag{7}$$

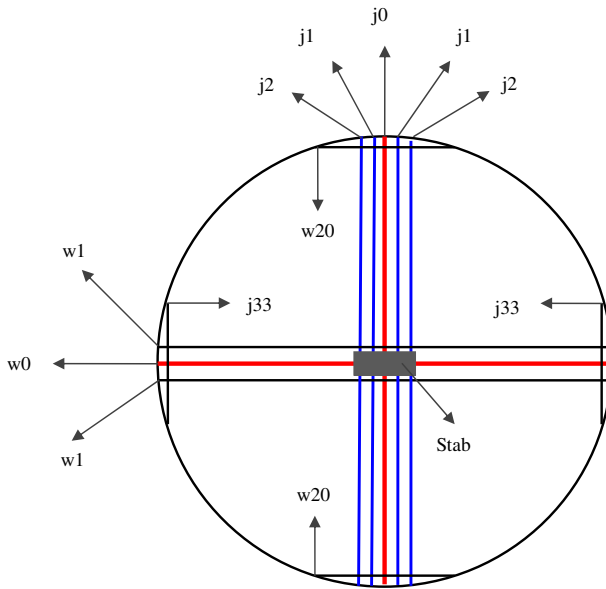


Fig. 11 Number of the warp and weft yarns in deformation region

For the warp yarns, “W” in Fig. 9 should be changed to “T”. Similarly, the length of half the j_0 yarns after elongating is

$$la_{j_0} = \frac{(2r - T)^2 + 4x^2}{4x} \cdot \arcsin\left(\frac{2x}{\sqrt{(2r - T)^2 + 4x^2}}\right) \tag{8}$$

The number of the warp and weft yarns and their distribution in the deformation region are shown in Fig. 11. There were 67 warp yarns and 41 weft yarns in total, and 6 of them were principal yarns, one in the weft direction and five in the warp direction. All the five principal yarns were regarded to be the same in the calculation. A quarter of the deformation region was chosen for calculation due to the symmetry of the structure. The length before and after elongating of the warp yarns are shown in Fig. 12.

The original length of the i th warp yarn is

$$l_{ji} = r \quad (0 \leq i \leq 2) \tag{9}$$

$$l_{ji} = \sqrt{r^2 - (i \cdot d_j)^2} \quad (3 \leq i \leq 33) \tag{10}$$

The length after elongating of the i th warp yarn is

$$la_{ji} = |\text{arc}AB|_j \quad (0 \leq i \leq 2) \tag{11}$$

$$la_{ji} = \sqrt{x_{sj}^2 + l_{ji}^2} \quad (3 \leq i \leq 33) \tag{12}$$

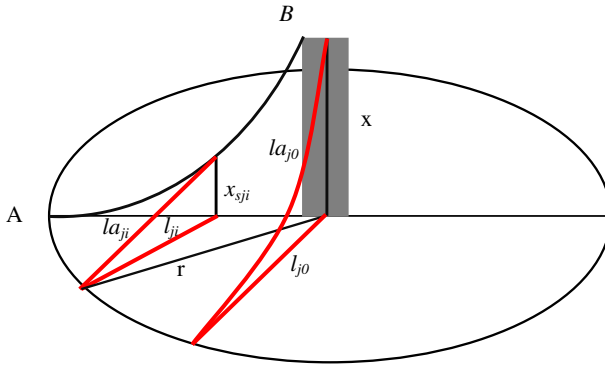


Fig. 12 Deformation of the warp yarns

The volume of the *i*th warp yarn is

$$V_{ji} = A_j \cdot l_{ji} \cdot 2 \tag{13}$$

The strain of the *i*th warp yarn could be expressed as:

$$\varepsilon_{ji} = \frac{la_{ji}}{l_{ji}} - 1 \tag{14}$$

The tensile strain energy stored in per cubic meter yarn is $\int_0^{\varepsilon_{\max}} \sigma(\varepsilon)d\varepsilon$. When the stab goes up by *x* (mm), the strain energy of the *i*th warp yarn could be written as follow:

$$e_{ji} = V_{ji} \cdot \int_0^x E_j \cdot \varepsilon_{ji} \cdot \frac{d}{dx} \varepsilon_{ji} dx \tag{15}$$

And the strain energy of the whole warp yarns could be obtained.

$$e_j = \sum_0^{33} V_{ji} \cdot \int_0^x E_j \cdot \varepsilon_{ji} \cdot \frac{d}{dx} \varepsilon_{ji} dx \tag{16}$$

The stab force borne by the warp yarns can be finally attained.

$$F_j = \frac{d}{dx} e_j \tag{17}$$

Similarly, the stab force sustained by the principal and secondary yarns in weft direction could be calculated.

3.3 Geometrical Model for the Resin

The TPU resin can be assumed as a piece of homogeneous membrane. With the stabbing process the TPU resin deformed into a conical shape as shown in Fig. 13a. In order to calculate the strain energy stored in the TPU, the surface area of the conical shape was approximately supposed to be the area of a circle with a radius of *r_a*. Figure 13b shows the area of the coating before and after deformation.

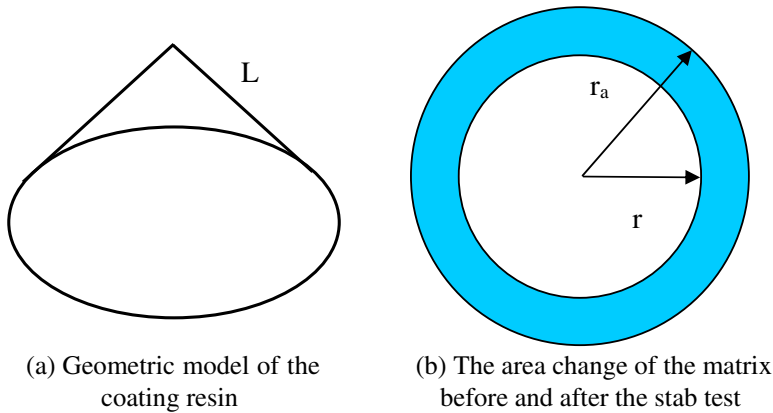


Fig. 13 Theoretical deformation of the TPU resin

3.4 Numerical Calculations for the TPU Resin

Similar to the analysis of the woven reinforcement, the stab force applied on the TPU resin could be calculated from Eqs. (15) to (21).

The surface area of the conical shape equals to that of the equivalent circle. Then the semi-diameter of the equivalent circle could be obtained as:

$$r_a = \sqrt{2 \cdot r \cdot L} \tag{18}$$

The strain of the radius could be expressed as:

$$\epsilon_r = \frac{r_a - r}{r} \tag{19}$$

The strain of the matrix could be calculated by integrating to ϵ_r

$$\epsilon_m = \int_0^{2\pi} \left(\frac{r_a - r}{r} \right) d\theta \tag{20}$$

The whole volume of the yarns is

$$V_y = 2 \cdot \left[\sum_1^{33} A_j \cdot l_{ji} \cdot 2 + \sum_1^{20} A_w \cdot l_{wi} \cdot 2 + r \cdot (A_j + A_w) \right] \tag{21}$$

There was nearly no space between the fabric and the resin, therefore, the volume of the matrix could be calculated by subtracting the volume of the yarns from the volume of the flexible woven composite.

$$V_m = \pi r^2 T_m - V_y \tag{22}$$

The strain energy stored in the matrix during the stab tests is

$$e_m = V_m \cdot \int_0^x E_m \cdot \epsilon_m \cdot \frac{d}{dx} \epsilon_m dx \tag{23}$$

Finally the force applied on the matrix could be calculated as follows:

$$F_m = \frac{d}{dx} e_m \tag{24}$$

3.5 Stab Force Applied on the Flexible Woven Composite

Strain energy stored in the flexible woven composite is the sum of the energy stored in the warp yarns, the weft yarns and the resin.

$$e_c = e_j + e_w + e_m \tag{25}$$

In all the above Equations, only x is the unknown variable, therefore the stab force could be finally deduced as an expression of x . The load–displacement curve could be obtained based on the expression.

$$F_c = \frac{d}{dx} e_c \tag{26}$$

Based on the Eq. (23), the applied force on the specimen could be calculated.

4 Results and Discussions

4.1 Load–Displacement Curves

As analyzed above, the stab force can be expressed as a function of the displacement of the stab. The displacement is 19 mm that when the specimen fractured in the experimental tests, so we assume the failure displacement for the specimen is 19 mm in the analytical model. Based on the maximum strain criterion the load–displacement curves of the specimen and its components could be obtained from the formulations in Sections 3.2, 3.4 and 3.5. All the results were calculated by using commercial software MAPLE 14.

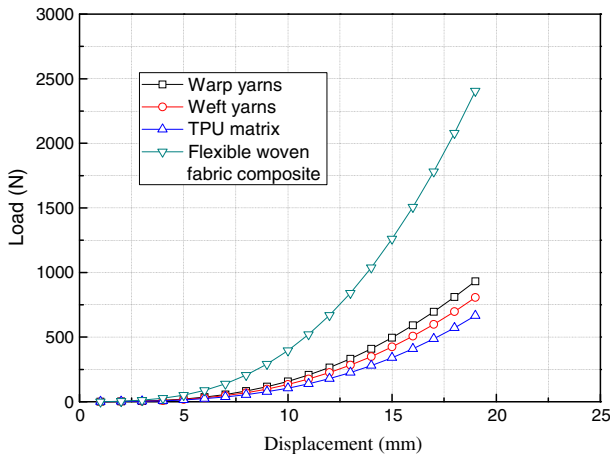


Fig. 14 Load–displacement curves of the calculation results

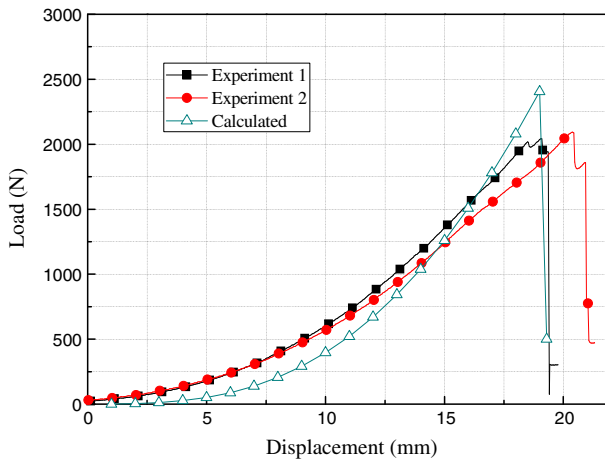


Fig. 15 Comparison between the experimental and the analytical results

Figure 14 shows the results of the warp yarns, weft yarns, the TPU resin and their combination during the stab process. It was observed that the most stab force was borne by the warp yarns, with the weft yarns being the second and the TPU matrix being the least. The fabric is to provide strength and dimensional stability to the flexible composite structure. The resin is mainly used to protect the fabric from being destroyed by the external environment and to provide the impermeable layer of the flexible woven composites.

Figure 15 compares the load–displacement curves of the specimen in experimental tests and analytical model, which showed a relative good agreement. The minor differences lay in the following two aspects: The initial modulus obtained from the analytical model was less than that of the experimental, while the failure strength corresponding to ultimate deflection in experimental tests was a little greater. The lower initial modulus in analytical may have been caused by not considering the friction between the fabric and the matrix and also between the weft and warp yarns. The lower stab strength in experimental could be ascribed to the pre-damage of the fabric during fabrication, the unevenness of the matrix and the imperfect bonding between the fabric and the matrix.

4.2 Maximum Strain and Force

The maximum strain and strength of the j0 yarn could be calculated according to formula (6), (9), (14) and (17). Table 4 indicates the results. The calculated value was lower than the tensile tested value which was similar to results found by Ghosh.[3]

Table 4 Calculated maximum strain and force of the principal yarn

Yarn	Maximum strain		Maximum force	
	Calculated	Experimental	Calculated	Experimental
Warp	6.56 %	12 %	280	480
Weft	6.56 %	14 %	173	300

While the locality results and analysis could not be obtained from the experimental tests, the analytical model helps a lot in analyzing the damage mechanism.

4.3 Damage Mechanisms and Failure Criteria

The TPU resin exhibits a good performance in the elongation with the failure strain being over 100 % which is much bigger than that of the PET yarn. The failure of the TPU is after that of the yarn and it damages rapidly because of the stress concentration, therefore the maximum stab strength is mainly depended on the reinforcement. The maximum strain criterion of the yarn should be considered as the failure criterion in the failure of the flexible woven composite. From the damage morphology in Fig. 6, it was seen that only the principal yarns were broken, hence the failure of the yarn just need to be focused on the No. 0 yarn (principal yarns) in the model. If the relationship between failure strain in stab and in tensile could be obtained, the maximum displacement of the stab could be predicted from formulas (8), (9) and (14). Then the maximum stab strength could be calculated according to the predicted results instead of the experimental maximum displacement. The maximum stab strain of the yarn could be used as the failure criterion of the flexible woven composite.

5 Conclusions

Flexible woven composites, as called coated woven fabrics, have been widely used in geotextiles and geomembranes because of the flexibility and impermeability. The flexible woven composite are easily undergone the stab or puncture damage during the service life which cause by the sharp objects or rocks. This paper presents an analytical model for predicting the stab resistance of the flexible woven composites. The stab performance of flexible woven composite was investigated both by experimental and analytical model. In experimental, the load–displacement curve was obtained. In addition, it was found that only the yarns contacted with the stab, named as the principal yarns, were broken. Based on the observations of the flexible composite stab deformation, an analytical model for the predicting the stab resistance was presented. The load–displacement curves of the flexible woven composite stabbed by a steel penetrator were obtained. From the comparisons of the stab force distributions, it was found that the principal yarns play an important role in stab resistance. The higher strength of yarns is recommended for improving the stab resistance. And also, with the increase of the weaving density, the numbers of the principal yarns will be increased and will also improving the stab resistance. From the load distribution analyses, the coating resin shares almost 30 % stab load. The high fracture strength resin will lead the high stab resistance flexible woven composites. We hope such an analytical model could be extended to the stab resistance design of flexible woven composites in efficient way. In addition, the analytical model has provided theoretical basis for simple structured flexible composites, and for the complicated structure the model need further improving.

Acknowledgments The authors acknowledge the financial supports from the National Science Foundation of China (Grant Numbers 11072058 and 11272087) and the Key-grant Project of Chinese Ministry of Education (No. 309014). The supports from Foundation for the Author of National Excellent Doctoral Dissertation of PR China (FANEDD, No. 201056), Shanghai Rising-Star Program (11QH1400100) and the Fundamental Research Funds for the Central Universities of China are also gratefully acknowledged.

References

1. Nguyen, C.T., Vu-Khanh, T., Lara, J.: Puncture characterization of rubber membranes. *Theor. Appl. Fract. Mech.* **42**(1), 25–33 (2004)
2. Kim, H., Nam, I.: Stab resisting behavior of polymeric resin reinforced p-aramid fabrics. *J. Appl. Polym. Sci.* **123**(5), 2733–2742 (2012)
3. Ghosh, T.K.: Puncture resistance of pre-strained geotextiles and its relation to uniaxial tensile strain at failure. *Geotext. Geomembr.* **16**(5), 293–302 (1998)
4. Mayo, J.B., et al.: Stab and puncture characterization of thermoplastic-impregnated aramid fabrics. *Int. J. Impact Eng.* **36**(9), 1095–1105 (2009)
5. Baucom, J.N., Zikry, M.A.: Evolution of failure mechanisms in 2D and 3D woven composite systems under quasi-static perforation. *J. Compos. Mater.* **37**(18), 1651–1674 (2003)
6. Yang, Y., et al.: Puncture deformation and fracture mechanism of oriented polymers. *J. Appl. Polym. Sci.* **124**(3), 2524–2536 (2012)
7. Tien, D.T., Kim, J.S., Huh, Y.: Evaluation of anti-stabbing performance of fabric layers woven with various hybrid yarns under different fabric conditions. *Fibers Polym.* **12**(6), 808–815 (2011)
8. Chen, J.M., et al.: Manufacturing and stab-resisting properties of compound fabric reinforced using recycled nonwoven selvages. In: Tunkasiri, T. (ed.) *Smart Materials*, pp. 417–420. Trans Tech Publications Ltd, Stafa-Zurich (2008)
9. Flambard, X., Polo, J.: Stab resistance of multi-layers knitted structures - (Comparison between para-aramid and PBO fibers). *J. Adv. Mater.* **36**(1), 30–35 (2004)
10. Brachman, R.W.I., Sabir, A.: Geomembrane puncture and strains from stones in an underlying clay layer. *Geotext. Geomembr.* **28**(4), 335–343 (2010)
11. Beiermann, B.A., Keller, M.W., Sottos, N.R.: Self-healing flexible laminates for resealing of puncture damage. *Smart Mater. Struct.* **18**(8), 085001 (2009)
12. Segreti, M., Rusinek, A., Klepaczko, J.R.: Experimental study on puncture of PMMA at low and high velocities, effect on the failure mode. *Polym. Test.* **23**(6), 703–718 (2004)
13. Hosur, M.V., et al.: Studies on the fabrication and stab resistance characterization of novel thermoplastic-kevlar composites. In: Lau, W., et al. (eds.) *Advanced Structural and Functional Materials for Protection*, pp. 83–92. Trans Tech Publications Ltd, Stafa-Zurich (2008)
14. Decker, M.J., et al.: Stab resistance of shear thickening fluid (STF)-treated fabrics. *Compos. Sci. Technol.* **67**(3–4), 565–578 (2007)
15. Termonia, Y.: Puncture resistance of fibrous structures. *Int. J. Impact Eng.* **32**(9), 1512–1520 (2006)
16. Lee, B.L., et al.: Penetration failure mechanisms of armor-grade fiber composites under impact. *J. Compos. Mater.* **35**(18), 1605–1633 (2001)
17. Sun, B., Wang, Y.X., Wang, P., et al.: Investigations of puncture behaviors of woven fabrics from finite element analyses and experimental tests. *Text. Res. J.* **81**(10), 992–1007 (2011)
18. Wang, P., Sun, B., Gu, B.: Comparison of stab behaviors of uncoated and coated woven fabrics from experimental and finite element analyses. *Text. Res. J.* **82**(13), 1337–1354 (2012)